Research Article | Vol. 30, No. 15 / 18 Jul 2022 / Optics Express 27912
Optics EXPRESS

Impact of homodyne receiver bandwidth and signal modulation patterns on the continuous-variable quantum key distribution

JIANQIANG LIU,[1,2] YANXIA CAO,[1,2] PU WANG,[1,2] SHUAISHUAI LIU,[1,2] ZHENGUO LU,[1,2] XUYANG WANG,[1,2] AND YONGMIN LI[1,2,*]

[1]*State Key Laboratory of Quantum Optics and Quantum Optics Devices, Institute of Opto-Electronics, Shanxi University, Taiyuan 030006, China*
[2]*Collaborative Innovation Center of Extreme Optics, Shanxi University, Taiyuan 030006, China*
[*]*yongmin@sxu.edu.cn*

Abstract: In continuous-variable quantum key distribution (CV-QKD), the key information are encoded on quadratures of the optical field, which are measured via balanced homodyne detector (BHD). The bandwidth of the BHD is one of key parameters for precise characterization of quantum states. We establish a theoretical model to analyze the impact of the BHD bandwidth and signal modulation patterns on the channel parameters estimation of CV-QKD systems. Based on the proposed model, the secure key rate of a practical CV-QKD system under different BHD bandwidths and signal modulation patterns are investigated. Our results show that insufficient BHD bandwidth will result in wrong estimate of the transmission loss and excess noise, which significantly affects the performance of CV-QKD systems. Given the BHD bandwidth, there exists an optimal signal repetition rate that maximizes the secure key rate. The BHD bandwidth requirement of the QKD system increases with the transmission distance for large duty cycle pulse. Furthermore, the root raised-cosine pulse signal modulation performs better than the square pulse signal modulation in general.

1. Introduction

Quantum key distribution (QKD)[1–3] enables two legitimate communication parties (Alice and Bob) to share information-theoretically secure key through an insecure quantum channel and an authenticated classical channel. Any eavesdropping behaviours aiming at the QKD system can be detected and the security is guaranteed by the laws of quantum mechanics rather than the complexity of mathematical algorithms. When combine with one-time pad encryption, secure and private communication can be realized. Various QKD protocols have been proposed and demonstrated during the past decades [4,5]. Many of them utilize discrete-variable (DV) of light fields as the carrier of the key information, such as the polarization or phase of single photon. The other protocols encode key information in continuous-variable (CV) of light fields, such as the amplitude and phase quadratures of quantized optical mode [6–8]. Due to its good compatibility with the standard optical telecommunication technologies and potential high secure key rate over metropolitan areas, significant progress have been seen in continuous-variable quantum key distribution (CV-QKD) [9–38].

For CV-QKD protocol based on Gaussian-modulated coherent states (GMCS) and homodyne detection [11], Alice prepares a train of Gaussian distribution coherent states and sends them to Bob. Bob randomly measures either amplitude or phase quadrature of the received states using the balanced homodyne detector (BHD). Based on the estimated secure key rate, Alice and Bob extract the secret key by using data error correction and privacy amplification. Recently, the composable security of the GMCS CV-QKD protocol has been proved against general attacks [28,39–41].

#461235 https://doi.org/10.1364/OE.461235
Journal © 2022 Received 14 Apr 2022; revised 14 Jun 2022; accepted 7 Jul 2022; published 15 Jul 2022

Optics EXPRESS

The GMCS CV-QKD protocol is considered to be a promising alternative in practical applications over metropolitan area secure networks. To date, a number of works have been implemented from laboratory system to field test. And the transmission distance has been extended to 202 km using ultralow-loss optical fiber [42]. Given the transmission distance, the secure key rate of the QKD system is mainly limited by the system excess noise and signal repetition rate. The former is caused by the imperfect state preparation [43], the Eve's eavesdropping, and the inaccurate measurement of the quantum state, etc. The latter is mainly limited by the BHD bandwidth and the speed of the classical data post-processing.

The design and construction of a wideband homodyne detector for time-domain quantum measurements has been reported [44]. By assuming a pulsed local oscillator (LO) with the pulse width much shorter than the time resolution of the detector, effective efficiency due to the electronic noise is derived. To get high secure key rate, Chi et al. discussed the induced excess noise by the electrical pulses overlap in time-domain BHD [45]. In [46], Tang et al. analyzed various noise sources at different clock rates and evaluated the performance of CV-QKD with fixed BHD bandwidth. Recently, the impact of receiver imbalances on the security of a heterodyne based CV-QKD system was reported in [47]. Although the finite bandwidth of the receiver is involved in the analysis, it remains constant. At present, the systematic investigation about the impact of the BHD bandwidth and signal modulation patterns on the performance of the CV-QKD system is still missing.

Since the design and fabrication of shot noise limited BHDs with very high bandwidth is technically challenging. In order to fully exploit the bandwidth of BHD and achieve high performance CV-QKD, in this paper, a theoretical model for the impact of the BHD bandwidth and signal modulation patterns on the channel parameter estimation of a CV-QKD system is proposed. In our model, we keep the pulse duration, pulse repetition period, and the detection bandwidth as independent variables, and choose the integration limits in a reasonable manner. Then, we analyze the performance of the CV-QKD system under the conditions of different BHD bandwidths and signal modulation patterns. For the fixed BHD bandwidth and transmission distance, the optimal signal repetition rates are derived.

The paper is organized as follows. In Sec. 2, we model the parameter estimation of the CV-QKD system with a finite-bandwidth BHD. In Sec. 3, we derive the secure key rate under finite-bandwidth BHD, and analyze the influences of the bandwidth on practical performance of a CV-QKD system. In Sec. 4, we analyze the parameter estimation of the CV-QKD system with a root raised-cosine pulse signal modulation and finite-bandwidth BHD. Finally, we present the conclusion in Sec. 5.

2. Influence mechanism of the BHD bandwidth on channel parameters estimation

2.1. BHD output under finite bandwidth

In Fig. 1, we show a typical schematic of the BHD with finite bandwidth. A signal mode is interfered with a phase reference mode (local oscillator, LO) at a 50:50 beam splitter. The two output fields emerging from the beam splitter are incident upon two photodiodes and the resulting photocurrents are subtracted. For BHD with infinite bandwidth, the photocurrent difference is proportional to the instantaneous quadrature of the signal field $\hat{x}(t,\theta) = \hat{a}_s^{\dagger}(t)e^{i\theta} + \hat{a}_s(t)e^{-i\theta}$, where $\hat{a}_s^{\dagger}(t)$ and $\hat{a}_s(t)$ denote creation and annihilation operators of the signal field, θ is the relative phase between the signal field and LO. Assume that the LO and signal have the same spatial mode, and their pulses duration and repetition period are s_0 and s, respectively, then the measured quadrature of the single pulsed signal mode $\hat{x}(\theta)$ defined by the spatial and temporal mode of the LO is given by

$$\hat{x}(\theta) = \int_0^{s_0} G\,|\alpha_L(t)|\,\hat{x}(t,\theta)\,dt, \tag{1}$$

Optics EXPRESS

where G denotes the optic-to-electronic gain factor and the strong LO has been treated as a classical field. We assume that the LO is a square pulse with $\alpha_L(t) = \alpha_L$, and omit θ in $\hat{x}(\theta)$ and $\hat{x}(t, \theta)$. In this case, Eq. (1) can be simplified as

$$\hat{x}=\frac{1}{\sqrt{s_0}}\int_0^{s_0}\hat{x}(t)\,dt. \tag{2}$$

To derive Eq. (2), we have set $G\alpha_L = 1/\sqrt{s_0}$ to normalize the variance of the vacuum field fluctuation.

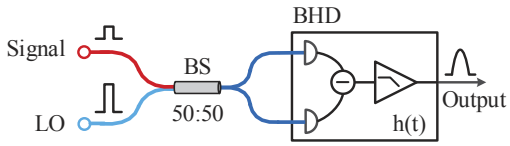

Fig. 1. Schematic of the balanced homodyne detection with finite bandwidth. BS, beam splitter; LO, local oscillator; $h(t)$, response function of the BHD.

For a practical BHD with finite bandwidth, we introduce a response function $h(t)$ [48,49], so that the measured quadrature of the single pulsed signal mode has the form

$$\hat{x} = \frac{1}{\sqrt{s_0}}\int_0^{s_1}\int_{-\infty}^{\infty} h(t-\tau)\hat{x}(\tau)\,d\tau dt, \tag{3}$$

where s_1 is the upper limit of the integral that depends on $h(t-\tau)$ and $\hat{x}(\tau)$. In the following, we will investigate in detail the channel parameters estimation under the finite-bandwidth BHD.

2.2. Estimation of the channel parameters in CV-QKD with finite-bandwidth BHD

In GMCS CV-QKD, Alice prepares a series of coherent states and their quadratures obey a centered bivariate Gaussian distribution in phase space. The amplitude quadrature of the signal mode is written as

$$\hat{x}_A(t) = x_A(t) + \hat{x}_{v1}(t), \tag{4}$$

where $\hat{x}_{v1}(t)$ is the quadrature of a vacuum field, and $x_A(t)$ denotes the Gaussian modulation signal with modulation variance of

$$V_A=\left\langle x_A^2\right\rangle, x_A=\frac{1}{\sqrt{s_0}}\int_0^{s_0} x_A(t)dt. \tag{5}$$

After transmitting through a quantum channel characterized by the transmittance T and excess noise ε, the signal mode measured by Bob's BHD has the form

$$\hat{x}_B(t) = \sqrt{\eta T}\left[\hat{x}_A(t) + \hat{x}_\varepsilon(t)\right] + \sqrt{1-\eta T}\hat{x}_{v2}(t) + x_{el}(t), \tag{6}$$

where $\hat{x}_\varepsilon$ is the quadrature of the auxiliary mode introduced by the eavesdropper, which satisfies $\langle\hat{x}_\varepsilon\rangle = 0$ and $\left\langle\hat{x}_\varepsilon^2\right\rangle = \varepsilon$, x_{v2} denotes the quadrature of a vacuum field which models the detection noise due to the imperfect quantum efficiency of the BHD, η and x_{el} denote the detection efficiency and electronic noise of Bob's BHD, respectively, and satisfy $\left\langle x_{el}^2\right\rangle = \upsilon_{el}$.

By introducing a noise operator $\hat{x}_N(t)$, Eq. (6) can be rewritten as

$$\hat{x}_B(t) = \sqrt{\eta T}x_A(t) + \hat{x}_N(t), \tag{7}$$

where $\hat{x}_N(t)$ is defined as

$$\hat{x}_N(t) = \sqrt{\eta T}x_{v1}(t)+\sqrt{\eta T}\hat{x}_\varepsilon(t) + \sqrt{1-\eta T}\hat{x}_{v2}(t) + x_{el}(t). \tag{8}$$

Hereafter, we consider only the impact of the closest signal pulse that dominates the impact on the current measurement results. In this case, the quadrature of the signal mode measured by

Optics EXPRESS

Bob's BHD is given by

$$\begin{aligned}\hat{x}_B &= \frac{1}{\sqrt{s_0}}\int_0^{s_1}\int_{-\infty}^{t} h(t-\tau)\hat{x}_B(\tau)d\tau dt \\ &= \frac{1}{\sqrt{s_0}}\int_0^{s_1}\int_0^{t} h(t-\tau)\hat{x}_B(\tau)d\tau dt + \frac{1}{\sqrt{s_0}}\int_0^{s_1}\int_{-s}^{0} h(t-\tau)\hat{x}_B(\tau)d\tau dt.\end{aligned} \tag{9}$$

In the second line of Eq. (9), we expand the integral to two terms. The first term denotes the contribution arising from the current signal pulse itself. The second term denotes the contribution arising from the closest signal pulse. In the case of infinite-bandwidth BHD, that means $h(t-\tau) = 2\delta(t-\tau)$, Eq. (9) can be rewritten as

$$\hat{x}_B = \frac{1}{\sqrt{s_0}}\int_0^{s_0} \hat{x}_B(t)dt. \tag{10}$$

After the send-receive and key sifting stages of the signal quantum states, Alice and Bob share a set of raw keys. By using random sampling, the quantum channel parameters T and ε can be estimated [21]. From Eqs. (4), (5), (7), (8), and (10), we have

$$\langle x_A\hat{x}_B\rangle = \frac{1}{s_0}\int_0^{s_0}\int_0^{s_0}\left\langle\sqrt{\eta T}x_A(t)x_A(t') + x_A(t)\hat{x}_N(t')\right\rangle dtdt', \tag{11}$$

$$\left\langle\hat{x}_B^2\right\rangle = \frac{1}{s_0}\int_0^{s_0}\int_0^{s_0}\left\langle(\sqrt{\eta T}x_A(t) + \hat{x}_N(t))(\sqrt{\eta T}x_A(t') + \hat{x}_N(t'))\right\rangle dtdt'. \tag{12}$$

Since the modulation signal $x_A(t)$ and the noise $\hat{x}_N(t)$ are independent of each other, Eqs. (11) and (12) can be calculated to be [43]

$$\langle x_A\hat{x}_B\rangle = \sqrt{\eta T}V_A, \tag{13}$$

$$\left\langle\hat{x}_B^2\right\rangle = \eta T(V_A+\varepsilon) + 1 + \upsilon_{el}. \tag{14}$$

In Eq. (14), the fluctuations of the vacuum field (shot noise for BHD) has been normalized. In terms of Eqs. (13) and (14), we can estimate the quantum channel parameters T and ε

$$T = \frac{\langle x_A\hat{x}_B\rangle^2}{\eta V_A^2}, \tag{15}$$

$$\varepsilon = \frac{\left\langle\hat{x}_B^2\right\rangle - 1 - \upsilon_{el}}{\eta T} - V_A. \tag{16}$$

At this stage, the secure key rate can be calculated based on the relevant parameters of the system. Then, the data post-processing technique (reconciliation and privacy amplification) is exploited to distill the secret key from the raw keys and guarantee the security.

In the above analysis, we have assumed that Bob performs measurement with an ideal BHD that has an infinite bandwidth. However, the practical BHDs always have a finite bandwidth, which inevitably distort the measurement outcomes and result in inaccurate parameter estimation. In the following part, the effect of the finite BHD bandwidth on the estimate of the quantum channel parameters is investigated.

Considering that the Butterworth filter is wildly used on the BHD, we assume that a fifth-order Butterworth low-pass filter is exploited hereafter, which has transfer function of the form [50]

$$H(s) = \frac{\omega_c^2}{\left(\omega_c s + \omega_c^2\right)\left[s^2 + 2\cos(\pi/5)\omega_c s + \omega_c^2\right]\left[s^2 + 2\cos(2\pi/5)\omega_c s + \omega_c^2\right]}, \tag{17}$$

where s=$i\omega$ and ω_c denotes the cut-off frequency of the filter. The impulse response $h(t)$ of the fifth-order Butterworth filter is given by the inverse Laplace Transform of its transfer function

Optics EXPRESS

$H(s)$

$$h(t)=\frac{1}{2\pi i}\int_{c-i\infty}^{c+i\infty}H(s)e^{st}ds. \tag{18}$$

By inserting Eq. (18) into Eq. (9), we can analyze the effect of the finite-bandwidth BHD on the channel parameters estimation. In Eq. (9), the upper limit of the integral for the variable t should be reasonably determined. For an ideal BHD with infinite bandwidth, the upper limit of the integral is exactly the optical pulse duration. For finite-bandwidth BHDs, it is not reasonable to integrate the electronic response pulses of the photodetection system just within the optical pulse duration. In this case, only partial electronic pulse signals are sampled and exploited, which will alter and distort the quadrature information of the signal field. By simulating the output electronic pulse shape of the BHD, the upper limit of the integral s_1 is selected as

$$s_1 = \begin{cases} s_0 + 2\pi/\omega_c, & s_0 + 2\pi/\omega_c < s \\ s, & s_0 + 2\pi/\omega_c \geq s \end{cases}. \tag{19}$$

In Eq. (19), the aliasing effects has been taken into account. Firstly, we consider the calibration of the shot noise and electronic noise. When the signal field is blocked and only the LO field is incident, the quadrature of the signal mode measured by Bob's finite-bandwidth BHD consists of the shot noise and electronic noise. In this case, applying Eqs. (8) and (9), the quadrature is given by

$$\hat{x}_{B1} = \frac{1}{\sqrt{s_0}}\left\{\int_0^{s_1}\int_0^t h(t-\tau)\hat{x}_{B1}(\tau)d\tau dt + \int_0^{s_1}\int_{-s}^0 h(t-\tau)\hat{x}_{B1}(\tau)d\tau dt\right\}, \tag{20}$$

where

$$\hat{x}_{B1}(\tau) = \hat{x}_v(\tau) + x_e(\tau). \tag{21}$$

It follows from Eqs. (20) and (21) that

$$\left\langle \hat{x}_{B1}^2 \right\rangle = \frac{1}{s_0}\left[A + A_1 + \upsilon_{el}(A_0 + A_2)\right], \tag{22}$$

where

$$\begin{aligned}
A_0 &= \left(\int_0^{s_1}\int_0^t\int_0^{t'} + \int_0^{s_1}\int_t^{s_1}\int_0^t\right)h(t-\tau)h(t'-\tau)d\tau dt' dt,\\
A &= \left(\int_0^{s_0}\int_0^t\int_0^{t'} + \int_{s_0}^{s_1}\int_0^{s_0}\int_0^{t'} + \int_{s_0}^{s_1}\int_{s_0}^{s_1}\int_0^{s_0} + \int_0^{s_0}\int_t^{s_1}\int_0^t\right)h(t-\tau)h(t'-\tau)d\tau dt' dt,\\
A_1 &= \int_0^{s_1}\int_0^{s_1}\int_{-s}^{-s+s_0} h(t-\tau)h(t'-\tau)d\tau dt' dt,\\
A_2 &= \int_0^{s_1}\int_0^{s_1}\int_{-s}^{0} h(t-\tau)h(t'-\tau)d\tau dt' dt,
\end{aligned} \tag{23}$$

where A and A_1 denote the contributions to the shot noise due to the current and the closest signal pulses, respectively, and A_0 and A_2 denote the contributions to the electronic noise due to the current and the closest pulses, respectively. In a similar manner, if we block both the signal and

Optics EXPRESS

LO fields, the variance of the electronic noise measured by the BHD has the form

$$\left\langle \hat{x}_{B2}^2 \right\rangle = \frac{1}{s_0} \upsilon_{el}(A_0 + A_2). \tag{24}$$

From Eqs. (22) and (24), the measured shot noise N_0 and electronic noise υ'_{el} (normalized to N_0) are given by

$$N_0 = \left\langle \hat{x}_{B1}^2 \right\rangle - \left\langle \hat{x}_{B2}^2 \right\rangle = (1/s_0)(A + A_1), \upsilon'_{el} = \frac{\left\langle \hat{x}_{B2}^2 \right\rangle}{N_0} = \upsilon_{el} \frac{A_0 + A_2}{A + A_1}. \tag{25}$$

By normalizing $\hat{x}_B$ to $\sqrt{N_0}$, Eqs. (13) and (14) are rewritten as

$$\left\langle \frac{x_A \hat{x}_B}{\sqrt{N_0}} \right\rangle = \frac{A_3 V_A \sqrt{\eta T}}{\sqrt{s_0(A + A_1)}}, \tag{26}$$

$$V_B = \frac{\left\langle \hat{x}_B^2 \right\rangle}{N_0} = \frac{A_3^2 + A_4^2}{s_0(A + A_1)} \eta T V_A + \eta T \varepsilon + 1 + \upsilon_{el} \frac{A_0 + A_2}{A + A_1}, \tag{27}$$

where $A_3 = (\int_0^{s_0} \int_0^t + \int_{s_0}^{s_1} \int_0^{s_0}) h(t - \tau) d\tau dt$ and $A_4 = \int_0^{s_1} \int_{-s}^{-s+s_0} h(t - \tau) d\tau dt$. Combine Eqs. (15), (16), (26), and (27), the estimated transmittance and excess noise of the quantum channel under finite-bandwidth BHD are derived as

$$T_1 = T \frac{A_3^2}{s_0(A + A_1)}, \tag{28}$$

$$\varepsilon_1 = \frac{s_0(A + A_1)}{A_3^2} \varepsilon + \frac{A_4^2}{A_3^2} V_A. \tag{29}$$

Figure 2 depicts the estimated channel parameters and normalized electronic noise as a function of the BHD bandwidth by using Eqs. (28) and (29). It is obvious that insufficient BHD bandwidth decreases the estimate value of the transmittance, whereas increases the estimate value of the excess noise and electronic noise. The physical mechanism is that the quadrature of signal quantum states measured by the finite-bandwidth BHD is incomplete and noisy due to the loss of the information at high frequency components and overlapping of adjacent signal pulses. This introduces noises on Bob's data and decreases the correlation between Alice's and Bob's data.

In the case of infinite-bandwidth BHD, the normalized electronic noise keeps constant. Although the electronic noise is estimated without quantum signal and LO, when the BHD bandwidth decreases from 5 GHz to around 1 GHz, the electronic noise power of current period declines due to the filtering effect, whereas the crosstalk of the adjacent pulse increases. The overall effect results the rise of the electronic noise. When the BHD bandwidth decreases further, the crosstalk of the adjacent pulse cannot compensate the rapid degradation of the current electronic noise, therefore the electronic noise starts to drop quickly. Above effect results in that the electronic noise has a peak value around 1 GHz and is dependent of duty cycle, as shown in Fig. 2(a).

Notice that estimation of the channel parameters is less sensitive for smaller duty cycle s_0/s when BHD bandwidth is larger than l.5 GHz (the repetition rate of the QKD system is 1 GHz). The transmittance can be accurately determined at BHD bandwidth above 3.5, 2 and 1.5 GHz for duty cycles of 0.8, 0.5 and 0.2, respectively. On the other hand, the excess noise can be accurately estimated when the BHD bandwidth is higher than 3.0, 2.0 and 2.0 GHz for duty cycles of 0.8, 0.5 and 0.2, respectively.

Optics EXPRESS

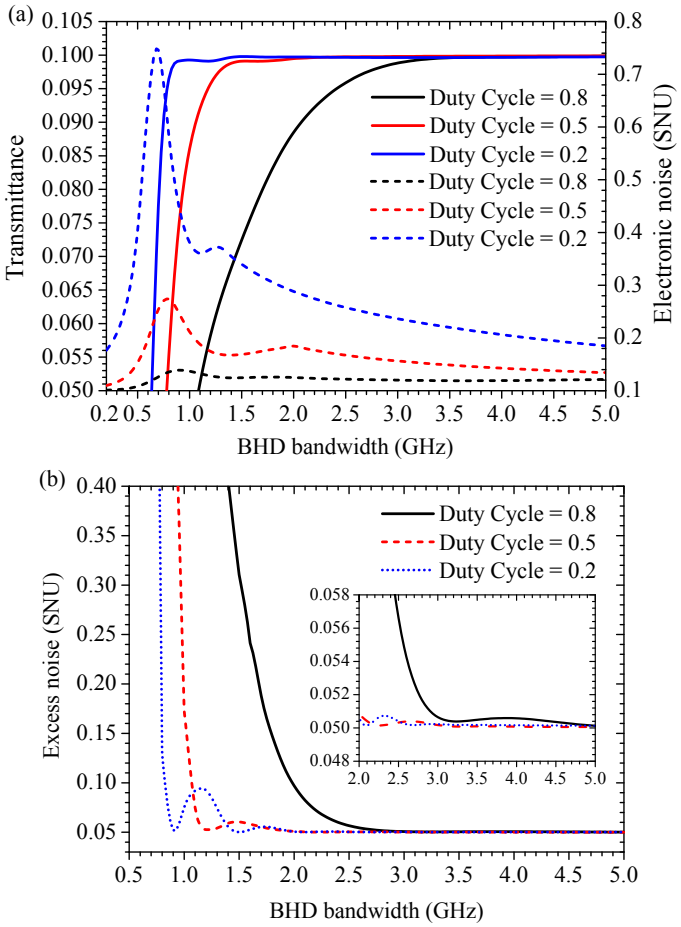

Fig. 2. Estimated transmittance and electronic noise (a), excess noise (b) of the CV-QKD system versus the BHD bandwidth at different duty cycles of 0.8, 0.5 and 0.2, when considering the influence of the closest signal pulse. In (a), the solid line denotes the transmittance and the dashed line denotes the electronic noise. SNU, shot noise unit. The parameters used for the simulations are: s = 1ns, $V_{\mathrm{A}} = 5$, $T = 0.1$, $\varepsilon = 0.05$, $\eta = 0.6$, and $\upsilon_{el} = 0.1$.

3. Performance analysis of the CV-QKD system with the finite-bandwidth BHD

The performance of a practical CV-QKD system is mainly characterized by the secure key rate and maximal transmission distance. Based on the estimated experimental parameters of the system V_{A}, T_1, ε_1, η, and υ'_{el}, Alice and Bob can estimate the secure key rate, which is expressed as [51]

$$K = \frac{n}{N}\left[\beta I_{AB}^{\epsilon_{PE}} - S_{BE}^{\epsilon_{PE}} - \Delta(n)\right]. \tag{30}$$

Here the finite-size effect has been considered. N denotes the total number of signals exchanged between Alice and Bob, n denotes the number of signals that is used to extract the final key, and the remaining $m = N - n$ signals are used for the parameter estimation. β is the reconciliation efficiency. $I_{AB}^{\epsilon_{PE}}$ and $S_{BE}^{\epsilon_{PE}}$ represent the Shannon mutual information and Holevo bound information compatible with the statistic fluctuations, except with probability ϵ_{PE}, respectively. $\Delta(n)$ is the

Optics EXPRESS

parameter related to the security of the privacy amplification, which has the form [51]

$$\Delta(n) \approx 7\sqrt{\frac{\log_2(2/\bar{\epsilon}\,)}{n}}, \tag{31}$$

where $\bar{\epsilon}$ is the probability of error during privacy amplification.

In the finite-size regime, the estimated channel parameters in Eqs. (28) and (29) are no longer the true channel parameters, but the expected values. We need to replace these parameters with their confidence intervals and find their boundary values that are most favorable for Eve. According to [51], the worst estimation of the unknown parameters T_1 and ε_1 are given by

$$T_{1,min} = \left(\hat{t} - z_{\epsilon_{PE}/2}\sqrt{\frac{\hat{\sigma}^2}{mV_A}}\right)^2/\eta, \quad \varepsilon_{1,max} = \left(\hat{\sigma}^2 + z_{\epsilon_{PE}/2}\frac{\hat{\sigma}^2\sqrt{2}}{\sqrt{m}} - 1 - \upsilon'_{el}\right)/\hat{t}^2. \tag{32}$$

where $z_{\epsilon_{PE}/2} = \sqrt{2}\mathrm{erf}^{-1}(1-\epsilon_{PE})$, and $\mathrm{erf}^{-1}(x)$ denotes the inverse function of the error function. The parameters $\hat{t}$ and $\hat{\sigma}^2$ are independent estimators, and from the theoretical perspective, we can assign them with the expected values $E(\hat{t}) = \sqrt{\eta T_1}$ and $E(\hat{\sigma}^2) = \eta T_1\varepsilon_1 + 1 + \upsilon'_{el}$.

Considering the statistic fluctuations, $I_{AB}^{\epsilon_{PE}}$ is given by

$$I_{AB}^{\epsilon_{PE}} = \frac{1}{2}\log_2\left(\frac{V_A + 1 + \hat{\chi}_{tot}}{1 + \hat{\chi}_{tot}}\right). \tag{33}$$

Here $\hat{\chi}_{tot} = \hat{\chi}_{line} + \chi_{hom}/\hat{T}_1$ represents the total noise referred to the quantum channel input, where $\hat{\chi}_{line} = 1/\hat{T}_1 - 1 + \hat{\varepsilon}_1$, $\chi_{hom} = \left[(1-\eta) + \upsilon'_{el}\right]/\eta$, $\hat{T}_1 = \hat{t}^2/\eta$, and $\hat{\varepsilon}_1 = (\hat{\sigma}^2 - 1 - \upsilon'_{el})/\hat{t}^2$. The Holevo bound $S_{BE}^{\epsilon_{PE}}$ is calculated by [15]

$$S_{BE}^{\epsilon_{PE}} = \sum_{i=1}^{2} G\left(\frac{\lambda_i - 1}{2}\right) - \sum_{i=3}^{5} G\left(\frac{\lambda_i - 1}{2}\right), \tag{34}$$

where $G(x) = (x+1)\log_2(x+1) - x\log_2 x$, $\lambda_i \geq 1$ are symplectic eigenvalues of the covariance matrices characterizing the quantum states

$$\begin{aligned} \lambda_{1,2}^2 &= \tfrac{1}{2}\left(A \pm \sqrt{A^2 - 4B}\right), \\ \lambda_{3,4}^2 &= \tfrac{1}{2}\left(C \pm \sqrt{C^2 - 4D}\right), \\ \lambda_5 &= 1, \end{aligned} \tag{35}$$

with the notations [15]

$$\begin{aligned} A &= (V_A+1)^2 + \left[\hat{T}_1(V_A + \hat{\varepsilon}_1) + 1\right]^2 - 2\hat{T}_1\left(V_A^2 + 2V_A\right), \\ B &= \left[(V_A+1)\left(\hat{T}_1\hat{\varepsilon}_1 + 1\right) - \hat{T}_1 V_A\right]^2, \\ C &= \frac{A\chi_{\mathrm{hom}} + (V_A+1)\sqrt{B} + \hat{T}_1(V_A + \hat{\varepsilon}_1) + 1}{\eta\hat{T}_1(V_A + \hat{\varepsilon}_1) + 1 + \upsilon'_{el}}, \\ D &= \frac{\sqrt{B}(V_A+1) + B\chi_{\mathrm{hom}}}{\eta\hat{T}_1(V_A + \hat{\varepsilon}_1) + 1 + \upsilon'_{el}}. \end{aligned} \tag{36}$$

At this stage, the lower bound of the secure key rate in the finite-size regime is given by [51]

$$K^L = \frac{n}{N}\left[\beta \cdot I_{AB}^{\epsilon_{PE}}(T_{1\,\mathrm{min}}, \varepsilon_{1\,\mathrm{max}}) - S_{BE}^{\epsilon_{PE}}(T_{1\,\mathrm{min}}, \varepsilon_{1\,\mathrm{max}}) - \Delta(n)\right]. \tag{37}$$

Using Eq. (37), we plot the secure key rate K^L (in unit of bits per pulse) versus the transmission distance at different BHD bandwidths, as shown in Fig. 3(a) and 3(b). The other numerical

Optics EXPRESS

simulation parameters are listed in Table 1. We find that the finite bandwidth obviously decreases the secure key rate and the transmission distance. Especially for duty cycle of 0.8, the effect is more evident. Compared with the ideal BHD with infinite bandwidth, the secure key rate and transmission distance are significantly degraded at bandwidth less than 2 GHz. Nevertheless, for bandwidth higher than 2 GHz at duty cycle of 0.5 and bandwidth higher than 3 GHz at duty cycle of 0.8, the effect of the BHD bandwidth on the channel parameters estimation is trivial. The secure key rate and the transmission distance are dramatically affected for bandwidth less than 2 GHz with duty cycle of 0.8.

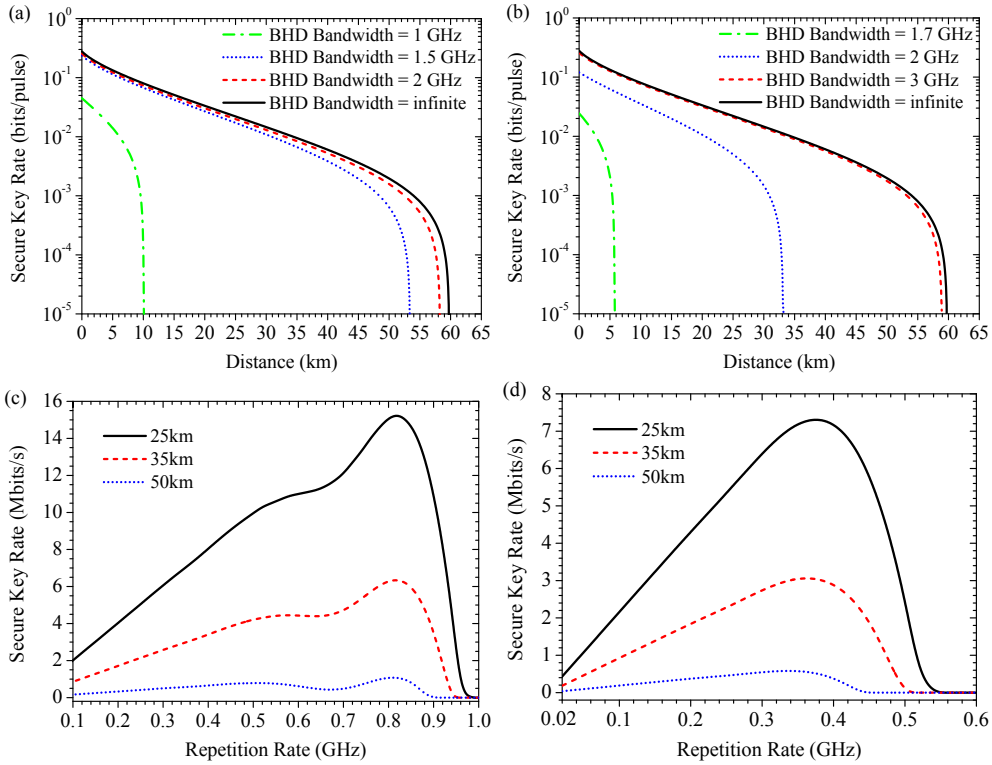

Fig. 3. (a) and (b) Secure key rate in unit of bits per pulse as a function of the transmission distance with different BHD bandwidth. (c) and (d) Secure key rate in unit of Mbits per second as a function of signal repetition rate of the system for transmission distances of 25, 35 and 50 km, respectively. The bandwidth of the BHD is 1 GHz. The duty cycles are 0.5 in (a), (c) and 0.8 in (b), (d), respectively. The other parameters are listed in Table 1.

Table 1. The simulation parameters for the performance analysis of the CV-QKD system. All the variances and noises are in shot noise unit.

s	V_A	T	ε	η	υ_{el}	β	N	m	$\bar{\epsilon}$
1ns	5	0.1	0.05	0.6	0.1	0.93	10^9	$10^9/2$	10^{-10}

Figure 3(c) and 3(d) show the secure key rate $K = R \cdot K^L$ (in unit of Mbits per second) as a function of signal repetition rate of the QKD system. Here R is the signal repetition rate of the QKD system, and the bandwidth of the BHD is 1 GHz. Three different transmission distances of 25, 35 and 50 km are investigated. We can see that the signal repetition rate exists an optimal value at each transmission distance, at this point, the secure key rate is maximized. When the

Optics EXPRESS

signal repetition rate R is much smaller than the BHD bandwidth, the signal quantum states can be precisely measured and the secure key rate K^L approaches to its maximum value. However, the small R inevitably decreases K. In contrast, when the signal repetition rate is close to the BHD bandwidth, although larger signal repetition rate is beneficial to the secure key rate K, the finite BHD bandwidth decreases the estimate value of the transmittance and increases the estimate value of the excess noise (Fig. 2). In this case, the value of secure key rate K^L drops quickly to zero, which results in that the secure key rate K drops to zero. Therefore, there exists an optimal R to maximize the secure key rate K. From Fig. 3(c), when the transmission distances are 25, 35 and 50 km, the optimal repetition rates are close and has the value of 0.82 GHz. From Fig. 3(d), when the transmission distances are 25, 35 and 50 km, the optimal repetition rates are 0.38, 0.36 and 0.34 GHz, respectively. We find that the large duty cycle pulse has a smaller optimal signal repetition rate, and the longer the transmission distances, the smaller the optimal signal repetition rate. The reason is that the secure key rate K at longer transmission distances is more sensitive to the excess noise and transmission distance of the quantum channel. Smaller signal repetition rate R results a lower estimate excess noise and higher estimate transmission distance.

In Fig. 3(c) and 3(d), the shape of the secure key rate lines is different for duty cycles of 0.5 and 0.8. For a duty cycle of 0.8, the secure key rate increases linearly with the repetition rate until it reaches a maximum. Nevertheless, we do not observe the same behaviour for a duty cycle of 0.5. The main reason is due to the different variations of the excess noise versus the BHD bandwidth for duty cycles of 0.5 and 0.8. As shown in Fig. 2(b), for duty cycle of 0.8, the excess noise monotonically increases as the BHD bandwidth reduces. However, for duty cycle of 0.5, the excess noise exhibits fluctuation as the BHD bandwidth decreases. In particular, the excess noise has an explicit peak at BHD bandwidth of around 1.5 GHz, which results in a valley point in secure key rate at the repetition rate of around 0.67 GHz in Fig. 3(c).

4. Performance of the CV-QKD system with a root raised-cosine pulse signal modulation and finite-bandwidth BHD

In the above sections, we have analyzed the performance of the CV-QKD system with the finite-bandwidth BHD. We have assumed that the signal modulation profile in each signal period is a square pulse, which is simple to implement in practice and has the form

$$x_A(t)=m_A,\ js \le t \le s_0 + js, j \in Z. \tag{38}$$

It is possible to utilize other signal modulation pattern to suppress the crosstalk between adjacent signal pulses in the QKD system. Here we assumed that a root raised-cosine pulse signal modulation pattern [47,52] with roll-factor $\gamma = 1$ [53] is employed for the Gaussian signal modulation

$$x_A(t)=m_A\sqrt{p(t)},\ p(t)=1-\sin[\frac{\pi(|t-js-s_0/2|-s_0/4)}{s_0/2}],\ js \le t \le s_0 + js, j \in Z. \tag{39}$$

In this case, we can derive the estimated transmittance, excess noise, and electronic noise of the CV-QKD system following the similar steps as above. The results have the same expression as Eqs. (28) and (29), and the definitions of A_0 and A_2 remain unchanged. However, the definitions of A, A_1, A_3 and A_4 are different, which are given by

$$\begin{aligned} A'=&(\int_0^{s_0}\int_0^{t}\int_0^{t'}+\int_{s_0}^{s_1}\int_0^{s_0}\int_0^{t'} \\ &+\int_{s_0}^{s_1}\int_{s_0}^{s_1}\int_0^{s_0}+\int_0^{s_0}\int_t^{s_1}\int_0^{t})h(t\text{-}\tau)h(t'\text{-}\tau)p(\tau)d\tau dt'dt \end{aligned}, \tag{40}$$

$$A_1'=\int_0^{s_1}\int_0^{s_1}\int_{-s}^{-s+s_0} h(t\text{-}\tau)h(t'\text{-}\tau)p(\tau)d\tau dt'dt, \tag{41}$$

Optics EXPRESS

$$A_3'=(\int_0^{s_0}\int_0^{t}+\int_{s_0}^{s_1}\int_0^{s_0})h(t-\tau)p(\tau)\,d\tau dt, \tag{42}$$

$$A_4'=\int_0^{s_1}\int_{-s}^{-s+s_0} h(t-\tau)p(\tau)d\tau dt. \tag{43}$$

Using Eqs. (28), (29), and (40–43), the estimated channel parameters with a root raised-cosine pulse signal modulation pattern versus the BHD bandwidth are illustrated in Fig. 4. Similar to the square pulse signal modulation pattern, the value of the excess noise is overestimated and the value of the transmittance is underestimated for finite BHD bandwidths. Compared with the square pulse signal modulation, the channel parameters estimation with a root raised-cosine pulse signal modulation are less affected by the BHD bandwidth and more accurate. The reason lies in that the root raised-cosine pulse signal modulation has a narrower frequency spectrum distribution range in frequency range in contrast to the square pulse signal modulation. Therefore, the finite bandwidth has a less impact on the fidelity of the measured signal and the crosstalk between adjacent signal pulses in general. From Fig. 4(a) and 4(c), as the bandwidth is higher than 3 GHz, the excess noise and transmittance with the root raised-cosine pulse signal modulation at duty cycle of 0.5 can be estimated with relative errors of $|T_1 - T|/T<0.1\%$ and $|\varepsilon_1 - \varepsilon|/\varepsilon<0.2\%$, respectively. For the duty cycle of 0.8 (Fig. 4(b) and 4(d)), as the bandwidth is higher than 3 GHz, the relative errors of the excess noise and transmittance are less than 0.3% and 0.4%, respectively.

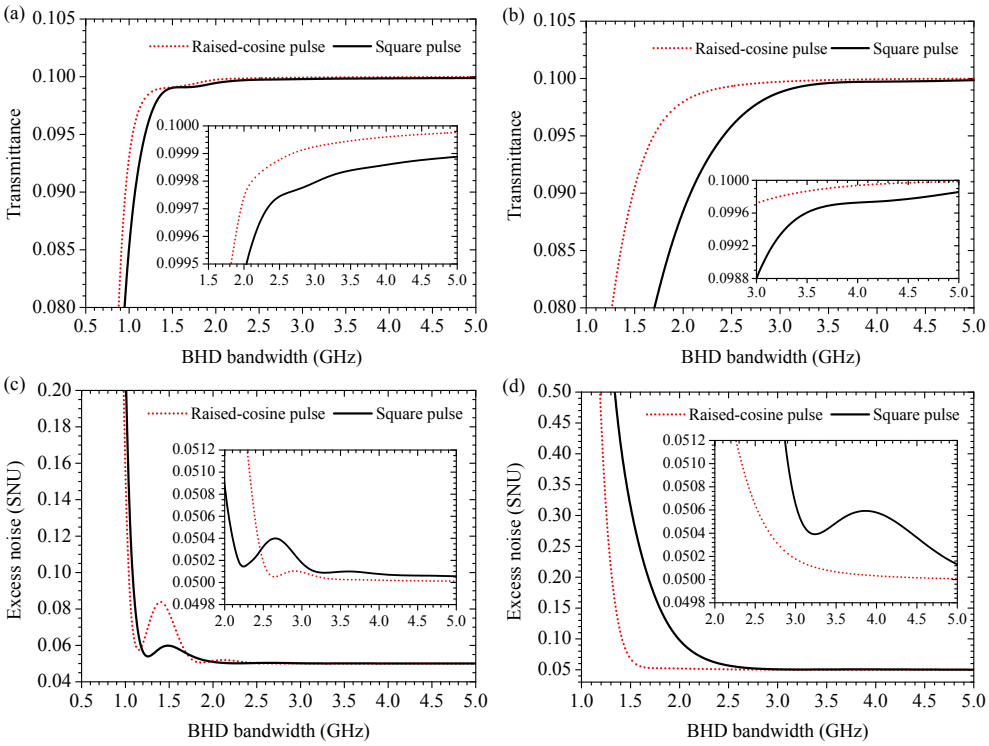

Fig. 4. Estimated channel transmittance (a), (b) and excess noise (c), (d) of the CV-QKD system vs the BHD bandwidth. Root raised-cosine pulse signal modulation pattern with the duty cycles of 0.5 ((a) and (c)) and 0.8 ((b) and (d)) are assumed to be employed for the Gaussian signal modulation. The other parameters used for the simulations are the same as in Fig. 2

Notice that the improvement with the root raised-cosine pulse signal modulation is more evident for the large duty cycle pulse signal modulation (see Fig. 4(b) and 4(d)). For duty cycle

Optics EXPRESS

of 0.8 and repetition period of 1 ns, the spectrum range of the root raised-cosine pulse almost cuts off at 2.5 GHz, however, the spectrum range of the square pulse is unbounded. As the BHD bandwidth is larger than 1.8 GHz, the root raised-cosine pulse can be measured with high fidelity and little crosstalk compared to the square pulse. In this case, the estimated excess noise and transmittance are almost unaffected.

Although the improvement of parameters estimation with root raised-cosine pulse signal modulation is not significant for large BHD bandwidth, it is useful for other CV-QKD protocols such as four-state modulation protocol and measurement-device-independent CV-QKD protocol, which are very sensitive to the channel excess noises.

5. Conclusion

In summary, we investigate the influence mechanism of the finite BHD bandwidth and signal modulation patterns on the performance of practical CV-QKD systems. To this end, the dependence model of the channel parameters estimation in CV-QKD on the BHD bandwidth and signal modulation patterns is established. Then, we derive the secure key rate in the finite-size regime under the condition of finite-bandwidth BHD. The results show that insufficient BHD bandwidth can significantly affect the channel parameters estimation and therefore the performance of the CV-QKD. We also find that the degree of influence depends on the exploited signal modulation patterns due to their different frequency spectrum distribution to be employed. The requirement of the BHD bandwidth for a CV-QKD system increases with the transmission distance for the large duty cycle pulse. The method developed is useful to analyze the impact of the homodyne bandwidth on other types of CV-QKD protocols. Our results can provide guidance for the design and optimization of high speed practical CV-QKD systems and may find other applications in the fields of quantum optics and quantum information.

Funding. National Key Research and Development Program of China (2016YFA0301403); National Natural Science Foundation of China (No. 11904219, No. 62175138); Key Research and Development Program of Guangdong Province (2020B0303040002); Aeronautical Science Foundation of China (20200020115001); Shanxi 1331KSC.

Disclosures. The authors declare no conflicts of interest.

Data availability. Data underlying the results presented in this paper are not publicly available at this time but may be obtained from the authors upon reasonable request.

References

1. N. Gisin, G. Ribordy, W. Tittel, and H. Zbinden, "Quantum cryptography," Rev. Mod. Phys. **74**(1), 145–195 (2002).
2. V. Scarani, H. Bechmann-Pasquinucci, N. J. Cerf, M. Dušek, N. Lütkenhaus, and M. Peev, "The security of practical quantum key distribution," Rev. Mod. Phys. **81**(3), 1301–1350 (2009).
3. H. K. Lo, M. Curty, and K. Tamaki, "Secure quantum key distribution," Nat. Photonics **8**(8), 595–604 (2014).
4. S. Pirandola, U. L. Andersen, L. Banchi, M. Berta, D. Bunandar, R. Colbeck, D. Englund, T. Gehring, C. Lupo, C. Ottaviani, J. L. Pereira, M. Razavi, J. S. Shaari, M. Tomamichel, V. C. Usenko, G. Vallone, P. Villoresi, and P. Wallden, "Advances in quantum cryptography," Adv. Opt. Photon. **12**(4), 1012–1236 (2020).
5. F. Xu, X. Ma, Q. Zhang, H. K. Lo, and J. W. Pan, "Secure quantum key distribution with realistic devices," Rev. Mod. Phys. **92**(2), 025002 (2020).
6. S. L. Braunstein and P. V. Loock, "Quantum information with continuous variables," Rev. Mod. Phys. **77**(2), 513–577 (2005).
7. C. Weedbrook, S. Pirandola, R. García-Patrón, N. J. Cerf, T. C. Ralph, J. H. Shapiro, and S. Lloyd, "Gaussian quantum information," Rev. Mod. Phys. **84**(2), 621–669 (2012).
8. E. Diamanti and A. Leverrier, "Distributing secret keys with quantum continuous variables: Principle, security and implementations," Entropy **17**(12), 6072–6092 (2015).
9. T. C. Ralph, "Continuous variable quantum cryptography," Phys. Rev. A **61**(1), 010303 (1999).
10. N. J. Cerf, M. Lévy, and G. V. Assche, "Quantum distribution of gaussian keys using squeezed states," Phys. Rev. A **63**(5), 052311 (2001).
11. F. Grosshans and P. Grangier, "Continuous variable quantum cryptography using coherent states," Phys. Rev. Lett. **88**(5), 057902 (2002).
12. F. Grosshans, G. V. Assche, J. Wenger, R. Brouri, N. J. Cerf, and P. Grangier, "Quantum key distribution using gaussian-modulated coherent states," Nature **421**(6920), 238–241 (2003).

Optics EXPRESS

13. C. Weedbrook, A. M. Lance, W. P. Bowen, T. Symul, T. C. Ralph, and P. K. Lam, "Quantum cryptography without switching," Phys. Rev. Lett. **93**(17), 170504 (2004).
14. A. M. Lance, T. Symul, V. Sharma, C. Weedbrook, T. C. Ralph, and P. K. Lam, "No-switching quantum key distribution using broadband modulated coherent light," Phys. Rev. Lett. **95**(18), 180503 (2005).
15. J. Lodewyck, M. Bloch, R. García-Patrón, S. Fossier, E. Karpov, E. Diamanti, T. Debuisschert, N. J. Cerf, R. Tualle-Brouri, S. W. McLaughlin, and P. Grangier, "Quantum key distribution over 25 km with an all-fiber continuous-variable system," Phys. Rev. A **76**(4), 042305 (2007).
16. B. Qi, L. L. Huang, L. Qian, and H. K. Lo, "Experimental study on the gaussian-modulated coherent-state quantum key distribution over standard telecommunication fibers," Phys. Rev. A **76**(5), 052323 (2007).
17. S. Pirandola, S. Mancini, S. Lloyd, and S. L. Braunstein, "Continuous-variable quantum cryptography using two-way quantum communication," Nat. Phys. **4**(9), 726–730 (2008).
18. A. Leverrier and P. Grangier, "Unconditional security proof of long-distance continuous-variable quantum key distribution with discrete modulation," Phys. Rev. Lett. **102**(18), 180504 (2009).
19. L. S. Madsen, V. C. Usenko, M. Lassen, R. Filip, and U. L. Andersen, "Continuous variable quantum key distribution with modulated entangled states," Nat. Commun. **3**(1), 1083 (2012).
20. F. Furrer, T. Franz, M. Berta, A. Leverrier, V. B. Scholz, M. Tomamichel, and R. F. Werner, "Continuous variable quantum key distribution: Finite-key analysis of composable security against coherent attacks," Phys. Rev. Lett. **109**(10), 100502 (2012).
21. P. Jouguet, S. Kunz-Jacques, A. Leverrier, P. Grangier, and E. Diamanti, "Experimental demonstration of long-distance continuous-variable quantum key distribution," Nat. Photonics **7**(5), 378–381 (2013).
22. C. Weedbrook, "Continuous-variable quantum key distribution with entanglement in the middle," Phys. Rev. A **87**(2), 022308 (2013).
23. S. Pirandola, C. Ottaviani, G. Spedalieri, C. Weedbrook, S. L. Braunstein, S. Lloyd, T. Gehring, C. S. Jacobsen, and U. L. Andersen, "High-rate measurement-device-independent quantum cryptography," Nat. Photonics **9**(6), 397–402 (2015).
24. V. C. Usenko and F. Grosshans, "Unidimensional continuous-variable quantum key distribution," Phys. Rev. A **92**(6), 062337 (2015).
25. T. Gehring, V. Händchen, J. Duhme, F. Furrer, T. Franz, C. Pacher, R. F. Werner, and R. Schnabel, "Implementation of continuous-variable quantum key distribution with composable and one-sided-device-independent security against coherent attacks," Nat. Commun. **6**(1), 8795 (2015).
26. D. Huang, P. Huang, H. Li, T. Wang, Y. Zhou, and G. Zeng, "Field demonstration of a continuous-variable quantum key distribution network," Opt. Lett. **41**(15), 3511–3514 (2016).
27. N. Walk, S. Hosseini, J. Geng, O. Thearle, J. Y. Haw, S. Armstrong, S. M. Assad, J. Janousek, T. C. Ralph, T. Symul, H. M. Wiseman, and P. K. Lam, "Experimental demonstration of gaussian protocols for one-sided device-independent quantum key distribution," Optica **3**(6), 634–642 (2016).
28. A. Leverrier, "Security of continuous-variable quantum key distribution via a gaussian de finetti reduction," Phys. Rev. Lett. **118**(20), 200501 (2017).
29. W. Liu, X. Wang, N. Wang, S. Du, and Y. Li, "Imperfect state preparation in continuous-variable quantum key distribution," Phys. Rev. A **96**(4), 042312 (2017).
30. X. Wang, W. Liu, P. Wang, and Y. Li, "Experimental study on all-fiber-based unidimensional continuous-variable quantum key distribution," Phys. Rev. A **95**(6), 062330 (2017).
31. F. Furrer and W. J. Munro, "Repeaters for continuous-variable quantum communication," Phys. Rev. A **98**(3), 032335 (2018).
32. F. Karinou, H. H. Brunner, C. H. F. Fung, L. C. Comandar, S. Bettelli, D. Hillerkuss, M. Kuschnerov, S. Mikroulis, D. Wang, C. Xie, M. Peev, and A. Poppe, "Toward the integration of cv quantum key distribution in deployed optical networks," IEEE Photonics Technol. Lett. **30**(7), 650–653 (2018).
33. N. Wang, S. Du, W. Liu, X. Wang, Y. Li, and K. Peng, "Long-distance continuous-variable quantum key distribution with entangled states," Phys. Rev. Applied **10**(6), 064028 (2018).
34. Y. Zhang, Z. Li, Z. Chen, C. Weedbrook, Y. Zhao, X. Wang, Y. Huang, C. Xu, X. Zhang, Z. Wang, M. Li, X. Zhang, Z. Zheng, B. Chu, X. Gao, N. Meng, W. Cai, Z. Wang, G. Wang, S. Yu, and H. Guo, "Continuous-variable QKD over 50 km commercial fiber," Quantum Science and Technology **4**(3), 035006 (2019).
35. Y. Zheng, P. Huang, A. Huang, J. Peng, and G. Zeng, "Practical security of continuous-variable quantum key distribution with reduced optical attenuation," Phys. Rev. A **100**(1), 012313 (2019).
36. S. Du, Y. Tian, and Y. Li, "Impact of four-wave-mixing noise from dense wavelength-division-multiplexing systems on entangled-state continuous-variable quantum key distribution," Phys. Rev. Applied **14**(2), 024013 (2020).
37. B. Qi, H. Gunther, P. G. Evans, B. P. Williams, R. M. Camacho, and N. A. Peters, "Experimental passive-state preparation for continuous-variable quantum communications," Phys. Rev. Applied **13**(5), 054065 (2020).
38. D. Dequal, L. Trigo Vidarte, V. Roman Rodriguez, G. Vallone, P. Villoresi, A. Leverrier, and E. Diamanti, "Feasibility of satellite-to-ground continuous-variable quantum key distribution," npj Quantum Information **7**(1), 3 (2021).
39. A. Leverrier, "Composable security proof for continuous-variable quantum key distribution with coherent states," Phys. Rev. Lett. **114**(7), 070501 (2015).
40. S. Pirandola, "Composable security for continuous variable quantum key distribution: Trust levels and practical key rates in wired and wireless networks," Phys. Rev. Res. **3**(4), 043014 (2021).

Optics EXPRESS

41. A. G. Mountogiannakis, P. Papanastasiou, B. Braverman, and S. Pirandola, "Composably secure data processing for Gaussian-modulated continuous-variable quantum key distribution," Phys. Rev. Res. **4**(1), 013099 (2022).
42. Y. Zhang, Z. Chen, S. Pirandola, X. Wang, C. Zhou, B. Chu, Y. Zhao, B. Xu, S. Yu, and H. Guo, "Long-distance continuous-variable quantum key distribution over 202.81 km of fiber," Phys. Rev. Lett. **125**(1), 010502 (2020).
43. P. Jouguet, S. Kunz-Jacques, E. Diamanti, and A. Leverrier, "Analysis of imperfections in practical continuous-variable quantum key distribution," Phys. Rev. A **86**(3), 032309 (2012).
44. R. Kumar, E. Barrios, A. MacRae, E. Cairns, E. Huntington, and A. Lvovsky, "Versatile wideband balanced detector for quantum optical homodyne tomography," Opt. Commun. **285**(24), 5259–5267 (2012).
45. Y. M. Chi, B. Qi, W. Zhu, L. Qian, H. K. Lo, S. H. Youn, A. I. Lvovsky, and L. Tian, "A balanced homodyne detector for high-rate gaussian-modulated coherent-state quantum key distribution," New J. Phys. **13**(1), 013003 (2011).
46. X. Tang, R. Kumar, S. Ren, A. Wonfor, R. Penty, and I. White, "Performance of continuous variable quantum key distribution system at different detector bandwidth," Opt. Commun. **471**, 126034 (2020).
47. D. Pereira, M. Almeida, M. Fac ao, A. N. Pinto, and N. A. Silva, "Impact of receiver imbalances on the security of continuous variables quantum key distribution," EPJ Quantum Technology **8**(1), 22 (2021).
48. B. Yurke, "Wideband photon counting and homodyne detection," Phys. Rev. A **32**(1), 311–323 (1985).
49. Z. Y. Ou and H. J. Kimble, "Probability distribution of photoelectric currents in photodetection processes and its connection to the measurement of a quantum state," Phys. Rev. A **52**(4), 3126–3146 (1995).
50. G. Ellis, "Control System Design Guide. (Butterworth-Heinemann, 2012)," Rev. Mod. Phys. **74**, 145–195 (2002).
51. A. Leverrier, F. Grosshans, and P. Grangier, "Finite-size analysis of a continuous-variable quantum key distribution," Phys. Rev. A **81**(6), 062343 (2010).
52. S. Kleis, M. Rueckmann, and C. G. Schaeffer, "Continuous variable quantum key distribution with a real local oscillator using simultaneous pilot signals," Opt. Lett. **42**(8), 1588–1591 (2017).
53. K. P. Ho and J. M. Kahn, "Spectrum of externally modulated optical signals," J. Lightwave Technol. **22**(2), 658–663 (2004).